14 *Chem. Mater.* **2011,** *23,* 14–20
DOI:10.1021/cm1027964

CHEMISTRY OF MATERIALS
Article

Vibrational Spectroscopy of Ca_2LnTaO_6 (Ln = lanthanides, Y, and In) and Ca_2InNbO_6 Double Perovskites

Anderson Dias,*[,†] Márcio M. Lage,[‡] L. Abdul Khalam,[§] Mailadil T. Sebastian,[§] and Roberto L. Moreira[#]

[†]*Departamento de Química, Universidade Federal de Ouro Preto, Campus Morro do Cruzeiro, ICEB II, Ouro Preto-MG, 35400-000, Brazil,* [‡]*Laboratório Interdisciplinar de Materiais Avançados, Universidade Federal de Itajubá (UNIFEI), Campus Itabira, Itabira-MG, 35900-373, Brazil,* [§]*Materials and Minerals Division, National Institute for Interdisciplinary Science and Technology, Trivandrum, 695 019, India, and* [#]*Departamento de Física, Universidade Federal de Minas Gerais, C.P. 702, Belo Horizonte-MG, 30123-970, Brazil*

Received September 28, 2010. Revised Manuscript Received November 18, 2010

Ca_2LnTaO_6 (Ln = lanthanides, Y, and In) and Ca_2InNbO_6 ceramics were prepared by the solid-state route, and their vibrational properties were investigated using Raman scattering and infrared spectroscopy. The correct crystal structure and phonon mode features for this lanthanide series in Ca-based double perovskites were determined using experimental data besides group-theoretical models. It was observed that the ceramics with Y, Er, and In exhibit orthorhombic, *Pbnm* (D_{2h}^{16}) structures, similarly to those previously observed in Ca_2LnNbO_6 ceramics, whereas the materials with La, Nd, Sm, Eu, Gd, Tb, and Ho show a monoclinic $P2_1/n$ (C_{2h}^5) structure, like Sr_2LnTaO_6 ceramics. Together with another two previous publications (Dias, A.; Khalam, L. A.; Sebastian, M. T.; Paschoal, C. W. A.; Moreira, R. L. *Chem. Mater.* **2006**, *18*, 214−220 and Dias, A.; Khalam, L. A.; Sebastian, M. T.; Lage, M. M.; Matinaga, F. M.; Moreira, R. L. *Chem. Mater.* **2008**, *20*, 5253−5259), the present results conclude the study for the A_2LnTaO_6 materials with alkaline-earth metals in the A-site, showing the changing in the crystalline structure as a function of the chemical environment.

Introduction

Perovskites are one of the most studied groups of materials, owing to their technological applications. An incredibly high versatility of structures and phases with totally different functions can be obtained depending upon the combination of chemical elements into the formula ABO_3.[1] Sometimes, multiple ion substitution in the perovskite lattice is required, which creates the well-known complex perovskites. These materials present pairs of unlike valence cations in proportions depending on their oxidation states and ionic radii.[1] In the last 50 years, a huge variety of compounds were studied in terms of their crystal chemistry aimed at emerging technological applications, such as ferroelectrics,[2] superconductors,[3] relaxors,[4] photonics,[5] catalysts,[6] and more recently microwave dielectrics.[7] In this respect, the ever-growing proliferation of the telecommunication technologies made an increasing demand for microwave dielectric ceramics.[7,8] These materials constitute the basic components in various communication and microwave systems providing very effective size reduction for microwave (MW) components. High dielectric constants (ε_r), minimum possible dielectric losses, and near-zero temperature stability of the resonant frequency (τ_f) are the basic requirements for MW applications, which are not fully attained by any compound. Even though a number of microwave resonator materials are available, the demand for new microwave dielectrics with multifunctional features is also increasing.[7]

In view of that, complex perovskites were studied due to open possibilities of tailoring the chemistry and consequently the parameters to meet the device requirements in microwave applications. It is well-known that the final properties are highly dependent on the nature of the cations present as well as on the structural features, including ordering and defects.[9] The most investigated complex perovskites are $Ba(Mg_{1/3}Ta_{2/3})O_3$ and $Ba(Zn_{1/3}Ta_{2/3})O_3$, as they possess excellent MW properties.[10] In spite of that, less attention has been paid to MW dielectric properties of $A_2B'B''O_6$, known as "double perovskites". Current investigations on these ceramics showed a number of temperature-stable MW dielectric

*Corresponding author. Tel. 55-31-3559-1716. E-mail: anderson_dias@iceb.ufop.br.

(1) Mitchell, R. H. *Perovskites modern and ancient*; Almaz Press: Ontario, 2002;Tejuca, L. G., Fierro, J. L. G., Eds. *Properties and applications of perovskite type oxides*; Marcel Decker: New York, 1993.
(2) Samara, G. A. *J. Phys.: Condens. Matter.* **2003**, *15*, R367.
(3) Blackstead, H. A.; Dow, J. D.; Harshman, D. R.; Yelon, W. B.; Chen, M. X.; Wu, M. K.; Chen, D. Y.; Chien, F. Z.; Pulling, D. B. *Phys. Rev. B* **2001**, *61*, 214412−1.
(4) Bokov, A. A.; Ye, Z. G. *J. Mater. Sci.* **2006**, *41*, 31.
(5) Wojtowicz, A. J.; Drozdowski, W.; Wisniewski, D.; Lefaucheur, J. L.; Galazka, Z.; Gou, Z. H.; Lukasiewicz, T.; Kisielewski, J. *Opt. Mater.* **2006**, *28*, 85.
(6) Osterloh, F. E. *Chem. Mater.* **2008**, *20*, 35.
(7) Reaney, I. M.; Iddles, D. *J. Am. Ceram. Soc.* **2006**, *89*, 2063.
(8) Subodh, G.; James, J.; Sebastian, M. T.; Paniago, R.; Dias, A.; Moreira, R. L. *Chem. Mater.* **2007**, *19*, 4077.
(9) Knapp, M. C.; Woodward, P. M. *J. Solid State Chem.* **2006**, *179*, 1076.
(10) Varma, M. R.; Raghunandan, R.; Sebastian, M. T. *Jpn. J. Appl. Phys.* **2005**, *44*, 298.

 Published on Web 12/08/2010

materials with potential new applications extended to the millimeter-wave range.[11−14] Among the double perovskites recently investigated, the series containing lanthanides in the B-sites besides niobium or tantalum present excellent microwave properties.[11−14] For these ceramics, the crystal structures are sometimes controversial: cubic, pseudocubic, tetragonal, orthorhombic, and monoclinic structures are frequently found in the literature.

Vibrational studies of the crystal structures and phonon features of complex perovskites using Raman scattering and infrared spectroscopy are reported by Dias et al.[8,14−17] These techniques are currently employed by these authors to investigate the behavior of the polar phonon modes for perovskite-type materials, once these modes determine completely the intrinsic dielectric contributions to the microwave response and are directly dependent on the crystalline structure. Thus, in order to study the potential of a given material to MW applications (resonators or filters), the knowledge of its polar phonon features is mandatory. Barium-,[17] strontium-,[18] and calcium-based[12] complex perovskites with lanthanides were previously studied from the point of view of their MW dielectric properties. Spectroscopic data can be found for Ba- and Sr-based ceramics,[14,17,19−23] for which different cubic, tetragonal, orthorhombic, and monoclinic structures were reported, depending on the lanthanide ionic radii.[18−23] In particular, A_2LnTaO_6 with barium or strontium in the A-site showed an interesting structure vs dielectric properties relationship.[14,20] In order to complete this lanthanide series, we focus now on the vibrational properties of Ca_2LnTaO_6 (Ln = lanthanides, Y, and In) and Ca_2InNbO_6 ceramics, the last series of double perovskites containing alkaline-earth elements. Raman scattering and far-infrared spectroscopy together with factor-group analysis were employed to show the relationship between crystal structure and vibrational modes, allowing us to contribute to the debate on the crystalline structure of this class of compounds.

Experimental Section

Ca_2LnTaO_6 (Ln = La, Nd, Sm, Eu, Gd, Tb, Ho, Y, Er, and In) and Ca_2InNbO_6 ceramics were prepared by the solid-state ceramic route. High purity $CaCO_3$ (99.9%, Aldrich Chemical, St. Louis, MO), rare-earth oxides (99.99%, Treibacher, Althofen, Austria), Nb_2O_5, and Ta_2O_5 (99.9%, Nuclear Fuel Complex, Hyderabad, India) were used as starting materials. Stoichiometric amounts of powder mixtures were ball-milled in distilled water medium using yttria-stabilized zirconia balls in a plastic container for 48 h. The slurry was dried, ground well, calcined at 1250 °C for 4 h, and then ground again in an agate mortar. They were then mixed with 3 wt % of polyvinyl alcohol (molecular weight of ≈22 000, BDH Lab Suppliers, England) and subsequently dried and ground well. Cylindrical pucks of about 7−9 mm height and 14 mm diameter were made by applying a pressure of 150 MPa. These compacts were then fired at 600 °C for 30 min to expel the binder before sintering at 1550−1600 °C for 4 h. Bulk densities of the sintered samples were measured using the Archimedes's method, and the results showed ceramics with values in the range of 97−99% of the theoretical value.

The crystal structure and phase purity of the sintered samples were studied by X-ray diffraction technique (XRD) using Cu Kα radiation (λ = 0.15418 nm) in a Rigaku diffractometer, with graphite monochromator and a nickel filter in the 2θ range of 10−70° (step 0.02°2θ). Raman spectra were collected in backscattering configuration using an Olympus confocal microscope attached to a triple-monochromator T64000 Jobin-Yvon spectrometer (objective 80×). Two different lines of an Ar^+ laser (514.5 and 488 nm, with effective 2 mW power at the sample's surface) were used as exciting lines. A liquid-N_2-cooled charge coupled device (CCD) detected the scattered light. The frequency resolution was better than 2 cm^{-1}, and the accumulation times were typically five collections of 60 s. Also, an Horiba/Jobin-Yvon LABRAM-HR spectrometer was used with the 632.8 nm line of a helium−neon laser (effective power of 6 mW at the sample's surface) as excitation source, diffraction gratings of 600 and 1800 grooves/mm, Peltier-cooled CCD detector, confocal Olympus microscope (100× objective), and experimental resolution of 1 cm^{-1} for 10 accumulations of 30 s. The obtained spectra were divided out by the Bose−Einstein thermal factor[24] before being fitted by a sum of Lorentzian lines. Polarized Raman spectra were carried out in sintered samples. Appropriate interference filters for rejecting laser plasma lines, edge filters for stray light rejection, polarizers, and half-wave plates were used.

Infrared reflectivity spectra were recorded in a Fourier-transform spectrometer (Bomem DA 8-02) equipped with a fixed-angle specular reflectance accessory (external incidence angle of 11.5°). In the mid-infrared region (500−4000 cm^{-1}), we used a SiC glow-bar lamp as infrared source, a Ge-coated KBr beamsplitter, and LN_2-cooled HgCdTe detector. In the far-infrared range (50−600 cm^{-1}), we employed a mercury-arc lamp, a 6 μm coated Mylar hypersplitter, and LHe-cooled Si-bolometer. The sample's surfaces were polished to an optical grade (0.25 μm) previously to the measurements. A gold mirror was used as reference. The data were collected at a pressure of 10^{-4} bar and a frequency resolution of 2 cm^{-1}. The reflectivity spectra were evaluated by means of standard Kramers−Krönig analysis and adjusted by an oscillator model. A generalized four-parameter oscillator model was used rather than the classical model to achieve a good fit with minimum number of physically meaningful oscillators.

Results

Figure 1 (inset) shows the XRD patterns for the sintered Ca_2LnTaO_6 (Ln = La, Nd, Sm, Eu, Gd, Tb, Ho, Y, Er, and In) and Ca_2InNbO_6 ceramics (herein designated as CRT).

(11) Khalam, L. A.; Sebastian, M. T. *Int. J. Appl. Ceram. Technol.* **2006**, *3*, 364.
(12) Khalam, L. A.; Sebastian, M. T. *J. Am. Ceram. Soc.* **2007**, *90*, 1467.
(13) Subodh, G.; Sebastian, M. T. *J. Am. Ceram. Soc.* **2007**, *90*, 2266.
(14) Dias, A.; Khalam, L. A.; Sebastian, M. T.; Paschoal, C. W. A.; Moreira, R. L. *Chem. Mater.* **2006**, *18*, 214.
(15) Surendran, K. P.; Sebastian, M. T.; Mohanan, P.; Moreira, R. L.; Dias, A. *Chem. Mater.* **2005**, *17*, 142.
(16) Dias, A.; Matinaga, F. M.; Moreira, R. L. *Chem. Mater.* **2007**, *19*, 2335.
(17) Moreira, R. L.; Khalam, L. A.; Sebastian, M. T.; Dias, A. *J. Eur. Ceram. Soc.* **2007**, *27*, 2803.
(18) Khalam, L. A.; Sebastian, M. T. *J. Am. Ceram. Soc.* **2006**, *89*, 3689.
(19) Ratheesh, R.; Wöhlecke, M.; Berge, B.; Wahlbrink, Th.; Haeuseler, H.; Rühl, E.; Blachnik, R.; Balan, P.; Santha, N.; Sebastian, M. T. *J. Appl. Phys.* **2000**, *88*, 2813.
(20) Dias, A.; Khalam, L. A.; Sebastian, M. T.; Lage, M. M.; Matinaga, F. M.; Moreira, R. L. *Chem. Mater.* **2008**, *20*, 5253.
(21) Petzelt, J.; Kamba, S. *Mater. Chem. Phys.* **2003**, *79*, 175.
(22) Zurmühlen, R.; Petzelt, J.; Kamba, S.; Voitsekhovskii, V.; Colla, E.; Setter, N. *J. Appl. Phys.* **1995**, *77*, 5341.
(23) Zurmühlen, R.; Petzelt, J.; Kamba, S.; Kozlov, G.; Volkov, A.; Gorshunov, B.; Dube, D.; Tagantsev, A.; Setter, N. *J. Appl. Phys.* **1995**, *77*, 5351.
(24) Hayes, W.; Loudon, R. *Scattering of light by crystals*; Wiley: New York, 1978.

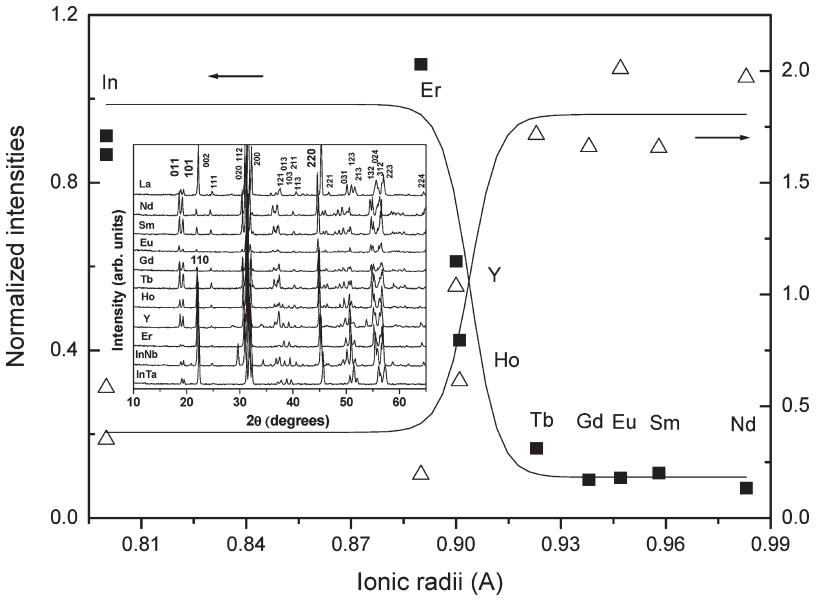

Figure 1. Normalized XRD intensities for the Ca_2LnTaO_6 (Ln = lanthanides, Y, and In) and Ca_2InNbO_6 ceramic samples. Full squares represent the ratio of orthorhombic peaks (110)/(220), while open triangles mean [(011) + (101)]/(220). Indeed, the (220) reflection would be indexed as (022) in the orthorhombic phase, with no consequence on the present results. Inset: XRD raw data for all materials (superlattice reflections are represented by the (111) and (113) planes).

The data for the sample with La were indexed by the most intense peaks (relative intensity higher than 5%) based on the monoclinic symmetry, space group $P2_1/n$.[25−27] Two weak additional lines, (111) and (113) planes, are indicative of the presence of a supercell in all investigated compounds investigated. It was observed that, as the ionic radii of the Ln elements increase (from In to La), the reflection peaks shift toward the low-angle side (higher lattice parameters). The results were similar to those observed in the analogous Ca_2LnNbO_6 materials.[12] For these ceramics, an orthorhombic structure for ceramics with lower ionic radii (Dy−In) and a monoclinic cell for La−Tb samples were reported. The main differences between these structures are a strong, very intense peak at around 22°2Θ, which corresponds to the (110) plane for the orthorhombic structure (absent in the monoclinic phase) and two weak peaks around 19°2Θ, which are related to the (011) and (101) planes of the monoclinic structure. For our samples, the XRD data were interpreted in terms of relative intensities of those peaks in all samples by calculating their normalized intensities relatively to the intense reflection around 45°2Θ, which is indexed as (220) in the monoclinic phase or (022) in the orthorhombic one. The results are displayed in Figure 1, where full squares give the normalized intensities of the orthorhombic (110) reflections and open triangles give the normalized intensities of the sum of the intensities of the monoclinic (011) and (101) peaks. This figure shows that we have predominantly orthorhombic structures for cations with lower ionic radii (Y, Er, and In) and monoclinic structures for the other ceramics (La, Nd, Sm, Eu, Gd, Tb, and Ho).

Raman analyses were carried out at room-temperature in all Ca_2LnTaO_6 and Ca_2InNbO_6 materials, and the results are displayed in Figure 2. As it can be seen, dissimilar spectral profiles are clearly observed, which indicates that the ceramics likely occur in different crystalline structure.

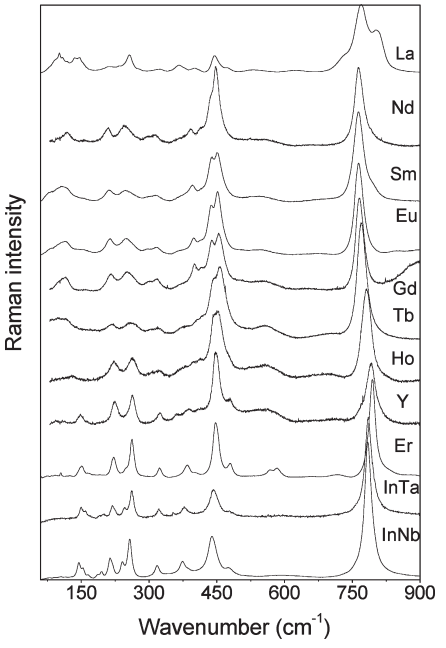

Figure 2. Room temperature Raman spectra for the Ca_2LnTaO_6 (Ln = lanthanides, Y, and In) and Ca_2InNbO_6 complex perovskites.

All samples were submitted to different Raman excitation lines because strong electronic transitions appeared for some conditions. The final spectra shown in Figure 2 represent the best results obtained using the blue line (488 nm) for Eu, Gd, Er, and In; green line (532 nm) for Ho and Yb; and the red line (632.8 nm) for La, Nd, Sm, and Tb. Dominating bands located at 150−300, 450, and 780 cm^{-1} are present in the samples, which were previously observed in similar 1:1 ordered ceramics.[14,17,20] The first difference between CRT samples and the previously investigated Sr-based ceramics,[20] which exhibited a monoclinic structure, is the absence of the sharp and intense set of splitted bands in

the range 100−200 cm^{-1}. A first tentative to explain this result could be accomplished by comparing with the previously reported ceramics with Ba and Sr.[14,17,20] Ba samples showed a very intense band around 100 cm^{-1} in both cubic and tetragonal structures,[14] while Sr-based materials showed a set of low-intensity, splitted bands in the same frequency region as a consequence of their ordered monoclinic structures.[20] As a first approximation, we think that the absence or even the presence of very low-intensity bands in this frequency range could be due to a local cationic disorder in the A-site. Because of the large number of visualized modes, a detailed investigation is mandatory and a correct assignment can be achieved only after theoretical considerations and fitting procedures, which will be presented below.

As a general trend, the Raman bands of all CRT ceramics show increasing wavenumbers from La to In, which is a consequence of decreasing ionic radii in this sequence, leading to a contracted unit-cell and, then, to stronger ionic bonds. Two similar patterns can be visualized: one for samples with small ionic radii (In, Er, and Y) and thinner bands and the other for samples with larger ionic radii (Ho, Tb, Eu, Gd, Sm, Nd, and La), which show broader, superimposed bands. Within each group, no relevant variation in frequency besides those due the lanthanide contraction was observed for bands below 600 cm^{-1}, which are related to Ca vibrations and are insensitive to chemical substitution on B-sites.[8,14−17] This result weakens the hypothesis for a cationic intersubstitution in A-sites in these samples, which would influence the wavenumbers and widths of these modes. While the mode centered at 540−580 cm^{-1} can be assigned as the F_{2g} stretching mode (ν_2 for a free octahedron), the set of modes centered at 430−440 cm^{-1} corresponds to the bending modes (ν_5 for a free octahedron). The region below 300 cm^{-1} is normally affected by composition (external modes), but no change was observed probably due to invariance of the cation on B″-site (Ta/Nb) in the studied samples. For frequencies above 650 cm^{-1}, a significant shift to lower frequencies was detected as a function of the rare-earth ion, from Y or Ho to La, which could indicate a cationic intersubstitution in these samples. The frequency range 700−900 cm^{-1} represents the vibrations of the oxygen octahedra with Ln/Ta cations on their interior. Changes in the composition will affect the modes, especially the A_g(O) peaks at 780−800 cm^{-1} (total symmetric stretching of the TaO_6 octahedra or the ν_1 mode for a free octahedron).

Ideal simple perovskite ($Pm\bar{3}m$) presents no-active first-order Raman phonons and only three infrared-active modes, while complex cubic perovskites of general formula $A_2B'B''O_6$ show four Raman-active modes ($A_{1g} \oplus E_g \oplus 2F_{2g}$), along with another four infrared-active bands ($4F_{1u}$), belonging to the $Fm\bar{3}m$ group. Ba-based samples studied in a previous publication were found to be cubic ($Fm\bar{3}m$) and tetragonal, space group $I4/m$, which exhibits nine Raman-active modes ($3A_g \oplus 3B_g \oplus 3E_g$) and nine infrared bands ($4A_u \oplus 5B_u$).[14] Ba_2LnTaO_6 materials (Ln = La, Nd, and Sm) were studied by Moreira et al.[17] and an orthorhombic structure $Pbnm$ (D_{2h}^{16}) was identified, which presented 24 Raman-active bands ($7A_g \oplus 5B_{1\,g} \oplus 7E_{2\,g} \oplus 5B_{3\,g}$) and 25 infrared-active modes ($9B_{1u} \oplus 7B_{2u} \oplus 9B_{3u}$). Sr-based materials were also studied[20] and exhibited a monoclinic structure, space group $P2_1/n$. This structure presents 24 Raman-active phonon modes ($12A_g \oplus 12B_g$) and 33 infrared-active modes ($17A_u \oplus 16B_u$). Our CRT samples investigated in the present work are expected to be orthorhombic or monoclinic in the same space groups of Ba_2LnTaO_6 or Sr-based samples, respectively. Thus, identical procedures employed in the previous publications were carried out, and careful fittings of the Raman spectra were done. The results for a typical monoclinic sample (Ca_2LaTaO_6) are displayed in Figure 3. The final fitting (red line in Figure 3) was obtained through a sum of 24 Lorentzian lines (blue lines in Figure 3), in perfect agreement with the theoretical predictions for monoclinic materials. Similar fittings with 24 bands could be obtained for all other CRT ceramics, irrespective of their crystal structure, once orthorhombic structure was also foreseen in 24 Raman modes, which are presented in the Supporting Information. Figure 3 also presents the parameters, after deconvolution, of the spectrum of Ca_2LaTaO_6, i.e., wavenumbers (ω, cm^{-1}) and full width at half-maxima (γ, cm^{-1}) for the phonon modes identified from the experimental data. The current Raman-spectroscopic results lead us to conclude that the correct structure for the Ca_2LnTaO_6 and Ca_2InNbO_6 perovskites appears to be dependent on the cation radius: La, Nd, Sm, Eu, Gd, Tb, and Ho ceramics crystallize in a monoclinic $P2_1/n$ (C_{2h}^5) structure, while Y, Er, and In ceramics present an orthorhombic $Pbnm$ (D_{2h}^{16}) structure, both with 24 Raman-active bands, according to factor-group analysis.

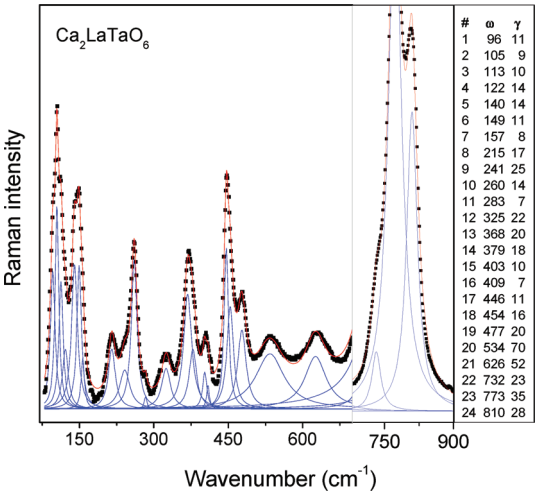

Figure 3. Raman spectra for Ca_2LaTaO_6 ceramics. Experimental data are in solid squares, while the fitting curve is the red line. Blue lines represent the phonon modes adjusted by Lorentzian curves. The obtained values for the wavenumbers and full widths at half maxima, in cm^{-1}, are displayed in the right section of the figure as numbered bands.

Now, the results of polarized Raman scattering will be presented. The inelastic light scattering intensities due to the Raman effect are proportional to the square of the elements of the polarizability tensor, a second-order tensor. Then, the base functions of the irreducible representation (i.r.) that contain the Raman-active modes have a quadratic form, i.e., they transform like the product of the Cartesian coordinates. When dealing with crystals, we take benefit of the crystal symmetry to assign the lattice

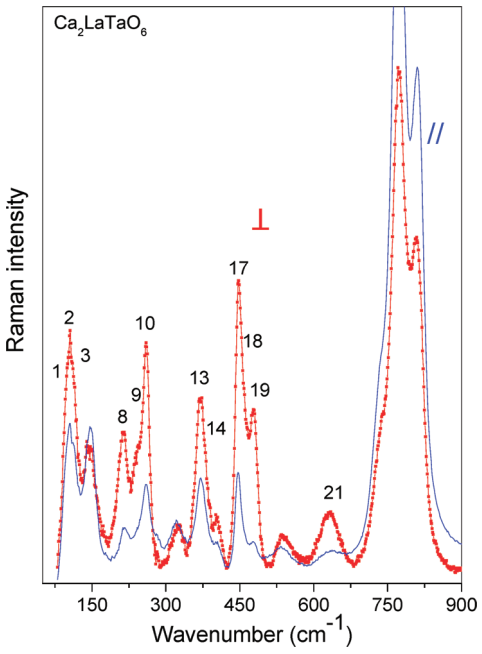

Figure 4. Polarized Raman scattering for the sintered Ca_2LaTaO_6 ceramic. Parallel- (//) and cross-polarized (⊥) configurations are indicated in blue and red lines, respectively. The twelve B_g modes resolved by the cross-polarized Raman scattering are indicated by numbered bands.

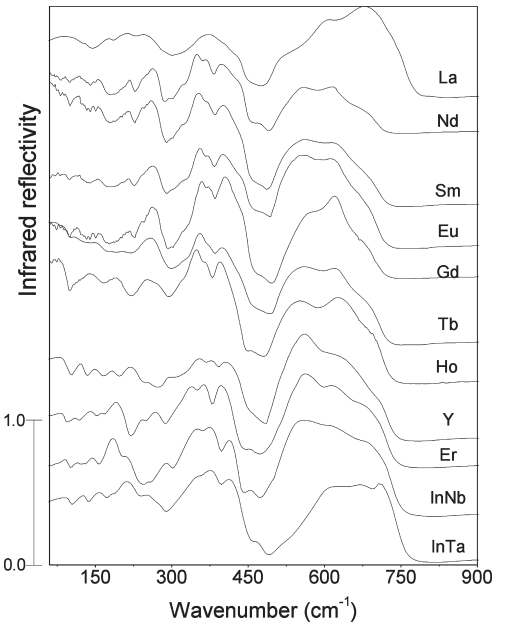

Figure 5. Infrared spectra for the Ca_2LnTaO_6 (Ln = La, Nd, Sm, Eu, Gd, Tb, Ho, Y, Er, and In) and Ca_2InNbO_6 ceramic materials.

vibrations to the different i.r.[24,28] However, in the case of ceramics, although the group-theory predictions remain valid, the symmetry of modes are generally mixed due to the random orientation of the small crystalline grains. In this work, we have used a confocal microscope with an objective of magnification of 80× or 100×, which allows the selection of an observation region as small as 2 μm on the sample surface or even inside the sample. All sintered samples were analyzed by polarized Raman spectroscopy. It is important to note that we do not know anything about the crystallographic axes inside the grains, which have also random orientation throughout the sample. By measuring the micro-Raman spectra of CRT sintered samples with cross-polarized light, we displaced the sample under the microscope looking for spectral changes. We observed that for some grains the spectra of parallel and crossed light became quite different, as exemplified in Figure 4 for the monoclinic Ca_2LaTaO_6 ceramics. For different grains, we always observed the relative strengthening of the bands numbered #1, #2, #3, #8, #9, #10, #13, #14, #17, #18, #19, and #21 with cross-polarized light, accompanied by the relative weakening of the remaining other bands. Therefore, we could assign these 12 Raman-active modes as belonging to the B_g i.r., while the 12 A_g modes are stronger in the parallel configuration, for this monoclinic structure. Similar results were obtained for the other samples with monoclinic structure, showing that although the total number of Raman modes for monoclinic and orthorhombic structures were the same, polarized spectra allowed one to determine undoubtedly the materials with monoclinic structure.

The infrared reflectivity spectra of the ceramic samples studied in the present work are displayed in Figure 5. It was observed that at least 13 well-defined modes for all materials can be clearly identified. Also, we can discern two different patterns for these materials: ceramics with In, Er, and Y present similar spectra, while ceramics containing Ho, Tb, Gd, Eu, Sm, Nd, and La could be grouped in a second type of reflectivity spectra. We believe that the infrared spectra can be described for two different crystal structures, in accordance with other experimental data. Again, the large number of predicted infrared bands for the structures considered here (33 for monoclinic and 25 for orthorhombic) and the similarity between the obtained spectra from previously studied Sr-based samples[20] make the analysis of the Ca-based samples difficult. However, we suppose that monoclinic structure holds for samples with Ho, Tb, Gd, Eu, Sm, Nd, and La, while orthorhombic structures are presented by Y, Er, and In materials. As a preliminary assignment, the bands above 450 cm^{-1} contain the ν_3 (F_{1u}) modes for a free octahedron, while the region 300–450 cm^{-1} includes the bending ν_4 modes. Below 300 cm^{-1}, the external (translational) modes dominate. A careful inspection of Figure 5 reveals the presence of several strong and weak bands, as well as shoulders in all samples. In view of that, a group-theory investigation was undertaken toward a better understanding of the crystal chemistry of these materials. The number of depicted bands will be known only after a precise fitting using the four-parameter semiquantum model[29] and a nonlinear least-squares program.[30] According to this model, the infrared phonon contributions to the

(25) Filipev, V. S.; Fesenko, E. G. *Soviet Phys. Crystallogr.* **1965**, *10*, 243.
(26) Galasso, F. S. *Structure, properties and preparation of perovskite type compounds*; Pergamon Press: Oxford, 1969.
(27) Khalam, L. A.; Thomas, S.; Sebastian, M. T. *J. Am. Ceram. Soc.* **2007**, *90*, 2476.
(28) Rousseau, D. L.; Bauman, R. P.; Porto, S. P. S. *J. Raman Spectrosc.* **1981**, *10*, 253.
(29) Gervais, F.; Echegut, P. In *Incommensurate phases in dielectrics*; Blinc, R., Levanyuk, A. P., Eds.; North Holland: Amsterdam, 1986; p 337.
(30) Meneses, D. D.; Gruener, G.; Malki, M.; Echegut, P. *J. Non-Cryst. Solids* **2005**, *351*, 124.

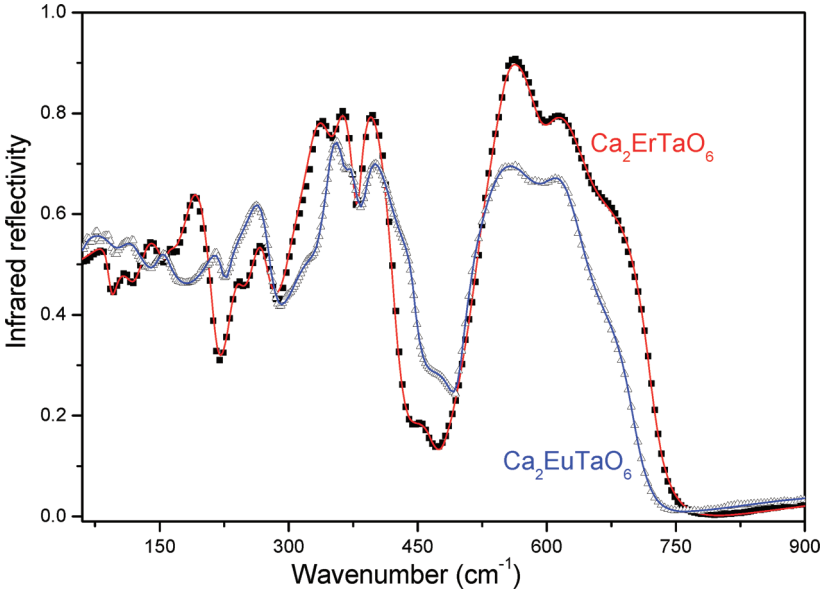

Figure 6. Infrared reflectivity spectra for the orthorhombic Ca_2ErTaO_6 (closed squares) and monoclinic Ca_2EuTaO_6 (open triangles) samples. The solid lines represent the fitting curves obtained using the four-parameter semiquantum model.

complex dielectric function $\varepsilon(\omega)$ are given by[29]

$$\varepsilon(\omega) = \varepsilon_\infty \prod_{j=1}^{N} \frac{\Omega_{j,LO}{}^2 - \omega^2 + i\omega\gamma_{j,LO}}{\Omega_{j,TO}{}^2 - \omega^2 + i\omega\gamma_{j,TO}} \qquad (1)$$

where ε_∞ is the dielectric constant due to the electronic polarization contribution, $\Omega_{j,LO}$ ($\Omega_{j,TO}$) and $\gamma_{j,LO}$ ($\gamma_{j,TO}$) are the frequency and damping of the j^{th} longitudinal (transverse) optical modes, respectively, and N is the number of polar phonons. At quasi-normal incidence, the dielectric function is related to the optical reflectivity R by the Fresnel formula:

$$R = \left| \frac{\sqrt{\varepsilon(\omega)} - 1}{\sqrt{\varepsilon(\omega)} + 1} \right|^2 \qquad (2)$$

Equations 1 and 2 were used to fit the experimental data for the Er and Eu ceramics (chosen as typical samples with orthorhombic and monoclinic structures, respectively), and the results are presented in Figure 6, as solid red (Er) and blue (Eu) curves. Then, we could obtain the wavenumbers and widths of the transverse (TO) and longitudinal (LO) infrared modes, which are listed in Table 1 for these samples. We note first the clear difference between the spectra profiles for the two structures. Also, 17 infrared modes can be adjusted for both Ca_2ErTaO_6 and Ca_2EuTaO_6 ceramics. For the orthorhombic samples (Er is the typical sample), the fitting results are close to the 25 infrared-active bands predicted by the group theory. Similarly, the results from fitting procedures for the monoclinic samples (Eu is the representative ceramic) indicate a perfect agreement between experimental data and factor-group analysis. Specifically, for these monoclinic ceramics, quasi-accidental degeneracy forbids the distinction between corresponding A_u and B_u modes, and also, only 17 infrared modes are observed instead of the 33 foreseen ones ($17A_u$, $16B_u$).[20,31−33] It is also worth noticing the similarity of the spectra of the Ca_2EuTaO_6 compound and those of Sr_2GdTaO_6 and $RE_2MgB''O_6$, which are derived from the fact that the vibrational modes come essentially from the MgO_6 and $B''O_6$ octahedra, as tentatively assigned in those references. Once the infrared modes were determined, the dielectric strengths of the individual j^{th} TO modes can be obtained (Table 1) by[29]

$$\Delta\varepsilon_j = \frac{\varepsilon_\infty}{\Omega_{j,TO}{}^2} \times \frac{\prod_k (\Omega_{k,LO}{}^2 - \Omega_{j,TO}{}^2)}{\prod_{k\neq j} (\Omega_{k,TO}{}^2 - \Omega_{j,TO}{}^2)} \qquad (3)$$

Table 1. Dispersion Parameters Calculated from the Fits of the Infrared Reflectivity Spectra of Ca_2ErTaO_6 and Ca_2EuTaO_6[a]

Ca_2ErTaO_6					Ca_2EuTaO_6				
$\Omega_{j,TO}$	$\gamma_{j,TO}$	$\Omega_{j,LO}$	$\gamma_{j,LO}$	$\Delta\varepsilon_j$	$\Omega_{j,TO}$	$\gamma_{j,TO}$	$\Omega_{j,LO}$	$\gamma_{j,LO}$	$\Delta\varepsilon_j$
92	20	94	12	2.301	71	33	80	44	7.844
112	47	120	27	6.781	86	33	101	61	2.330
137	28	138	29	2.661	115	33	117	86	0.277
138	33	158	15	4.663	153	20	153	30	0.039
159	14	163	50	0.111	220	33	225	15	1.101
187	24	216	24	3.669	229	28	230	68	0.084
238	19	244	29	0.595	262	31	280	30	2.120
264	22	279	33	1.270	320	47	332	40	1.591
307	35	311	52	0.737	347	18	366	16	1.479
324	27	350	29	2.155	368	14	382	24	0.130
355	25	378	17	0.374	389	22	435	84	0.355
383	16	428	32	0.233	442	29	447	24	0.020
459	56	471	34	0.204	491	77	494	25	0.121
524	25	541	54	1.129	507	29	513	96	0.280
541	32	594	45	0.019	527	60	600	97	0.619
599	43	649	79	0.056	606	62	642	92	0.030
659	88	722	30	0.045	678	93	704	42	0.058
ε_∞ = 3.7			ε_r = 27.0		ε_∞ = 3.73			ε_r = 22.2	

[a] The positions (Ω) and damping constants (γ) are given in cm^{-1}. $\Delta\varepsilon_j$ represents the dielectric strength of the j^{th} oscillator.

(31) Salak, A. N.; Khalyavin, D. D.; Ferreira, V. M.; Ribeiro, J. L.; Vieira, L. G. *J. Appl. Phys.* **2006**, *99*, 094104.
(32) Babu, G. S.; Subramanian, V.; Murthy, V. R. K.; Lin, I. N.; Chia, C. T.; Liu, H. L. *J. Appl. Phys.* **2007**, *102*, 064906.
(33) Babu, G. S.; Subramanian, V.; Murthy, V. R. K.; Moreira, R. L.; Lobo, R. P. S. M. *J. Appl. Phys.* **2008**, *103*, 084104.

The static (infrared) dielectric constant, which corresponds to the intrinsic MW dielectric constant, can be obtained by adding the dielectric strengths over all modes according to the equation:

$$\varepsilon_r = \varepsilon_\infty + \sum_{j=i}^{N} \Delta\varepsilon_j \quad (4)$$

The values of ε_r and ε_∞ for the sample with Er (orthorhombic) and Eu (monoclinic) are given in Table 1, along with the phonon modes parameters. A table with frequencies and damping constants after fitting procedures for the other ceramics investigated here are presented in the Supporting Information. Similarly to Sr-based ceramics previously studied,[20] the lower number of depicted infrared modes for Ca-based materials compared to the foreseen ones is due to the proximity between modes of different irreducible representations, which forbids their individual assessment by regular fitting procedures. Thus, the unloaded quality factors at the microwave region as obtained by Fourier transform infrared spectroscopy (FTIR) measurements were not calculated. In fact, in such cases, overestimated intrinsic quality factors due to to the dominance of extrinsic losses of different origins (polar species, microstructural defects, etc.) usually dominate over the intrinsic phonon response.[21−23]

The infrared reflectivity spectra displayed in Figure 5 were subjected to the Kramers−Krönig analysis (in fact, the integration region was 50−4000 cm^{-1}). The complex dielectric constant, $\varepsilon(\omega) = \varepsilon'(\omega) + i\varepsilon''(\omega)$, of each CRT material was calculated, and the imaginary part of $\varepsilon(\omega)$, denoted ε'', was investigated in detail. This optical function was studied because it gives the values of the TO-mode frequencies and damping constants. These values can be compared with those normally obtained from the fit with the advantage of studying individual phonon contributions without any physical inconsistency. Figure 7 shows the evolution of the ε'' spectra, as a function of the chemical substitution on B-site of the double perovskites, in the range of 50−900 cm^{-1}. It is clear that the materials belong to distinct structures: In, Er, and Y show thinner modes with similar pattern, while the other samples show another pattern with broader modes, similar to Raman results presented previously. Let us analyze the behavior of the individual modes as the lanthanide ion changed. The lower-frequency modes in Figure 7 (< 350 cm^{-1}) are the most important ones in view of their contribution to the dielectric and microwave properties. These sets of intense peaks represent the main vibrational modes and can be attributed to the $Ca-BO_3$ external vibration as well as to the vibrations for each LnO_6 and TaO_6 octahedra (O−Ln−O and O−Ta−O bending). Because the charge of Ta^{5+} is higher than that of Ln^{3+}, the force constant associated with the Ta−O vibration must be larger than that of the Ln−O vibration. As a consequence, Ln−O modes dominate the lower-frequency region of the spectra. Besides, higher Ln ionic radii (from In to La) lead to lower frequency modes. The most relevant information in the highest wavenumber range (600−900 cm^{-1}) concerns the contributions of TaO_6 and LnO_6 stretching vibrations to the optical and dielectric properties. As a general trend, the polar (infrared) modes decreased their frequencies and broadened for increasing Ln ionic radii, as expected.

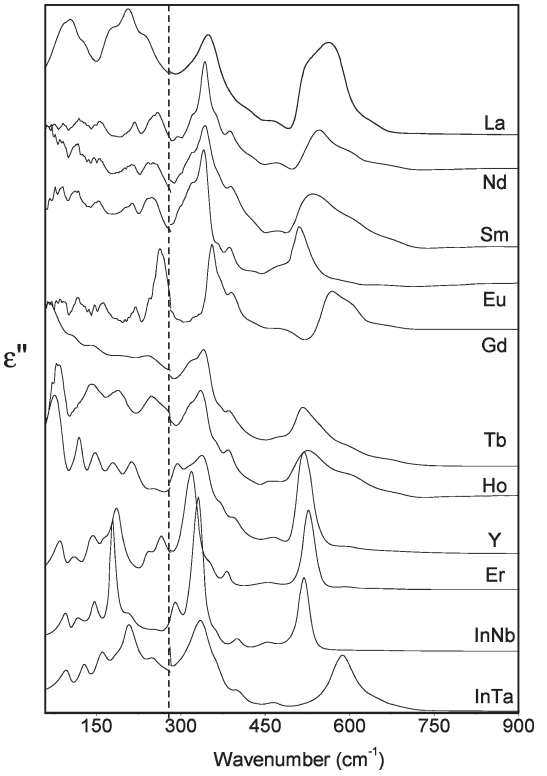

Figure 7. Imaginary part of the dielectric constant (ε'') calculated from Kramers−Krönig analyses for the Ca_2LnTaO_6 and Ca_2InNbO_6 materials, in the far-infrared region (50−1000 cm^{-1}). The dashed line centered at 290 cm^{-1} denotes a change in the intensity scale used for better visualization.

Conclusions

Ca_2LnTaO_6 (Ln = lanthanides, Y, and In) and Ca_2InNbO_6 ceramics were synthesized and studied by XRD, Raman scattering, and infrared spectroscopy. The results allowed us to determine the correct structure and phonon modes for the lanthanide series in Ca-based double perovskites at the light of group-theoretical models. Two different crystal structures can be inferred from the spectroscopic results based upon the spectra profile and symmetry rules: orthorhombic *Pbnm* (D_{2h}^{16}) for In, Er, and Y samples and monoclinic $P2_1/n$ (C_{2h}^{5}) for La, Nd, Sm, Eu, Gd, Tb, and Ho materials. These results conclude the study of A_2LnTaO_6 materials with alkaline-earth metals in the A-site, showing the change in their crystalline structure as a function of the cationic substitution. No noticeable evidence of cationic intersubstitution was found in the vibrational spectroscopic data of CRT materials.

Acknowledgment. The Brazilian authors acknowledge the financial support from CNPq, FINEP, and FAPEMIG. Indian authors are grateful to Council of Scientific and Industrial Research (CSIR, India). We also thank the researchers of LabCri-UFMG for their assistance with XRD analyses.

Supporting Information Available: Experimental Raman and far-infrared tables with fitting parameters, for all studied samples (PDF). This material is available free of charge via the Internet at http://pubs.acs.org.